THE EXPERIMENTAL AND SHELL MODEL APPROACH TO ^{100}Sn*

H. GRAWE[a], R. SCHUBART[b], M. GORSKA[c], K.H. MAIER[a],

J.B. FITZGERALD[a], J. HEESE[a], M. REJMUND[c], K. SPOHR[a],

the OSIRIS and NORDBALL collaborations

[a] Hahn-Meitner Institut
Glienicker Str. 100, D-141 Berlin, Germany
[b] II. Physikal. Institut, Universität Göttingen, Germany
[c] Institute of Experimental Physics, Warsaw University
Hoża 69, 00-681 Warsaw, Poland

(Received October 10, 1994)

The present status of experimental approach to ^{100}Sn and its shell model structure is given. New developments in experimental techniques, such as low background isomer spectroscopy and charged particle detection in 4π are surveyed. Based on recent experimental data shell model calculations are used to predict the structure of the single- and two-nucleon neighbours of ^{100}Sn. The results are compared to the systematics of Coulomb energies and spin-orbit splitting and discussed with respect to future experiments.

PACS numbers: 21.10.Sf, 21.60.Cs, 23.20.-g, 27.60.+j

1. Introduction

The doubly magic nucleus ^{100}Sn has attracted much attention in the past both in β^+/EC decay studies and in-beam experiments. More nuclear structure studies close to this last $N = Z$ doubly magic nucleus will be stimulated by the present detector developments following the recent first observation of ^{100}Sn [1, 2]. This paper presents the status of experimental studies with main emphasis on in-beam work, and the knowledge of the shell model structure around ^{100}Sn. In Fig. 1 the present experimental status is

* Presented at the XXIX Zakopane School of Physics, Zakopane, Poland, September 5–14, 1994.

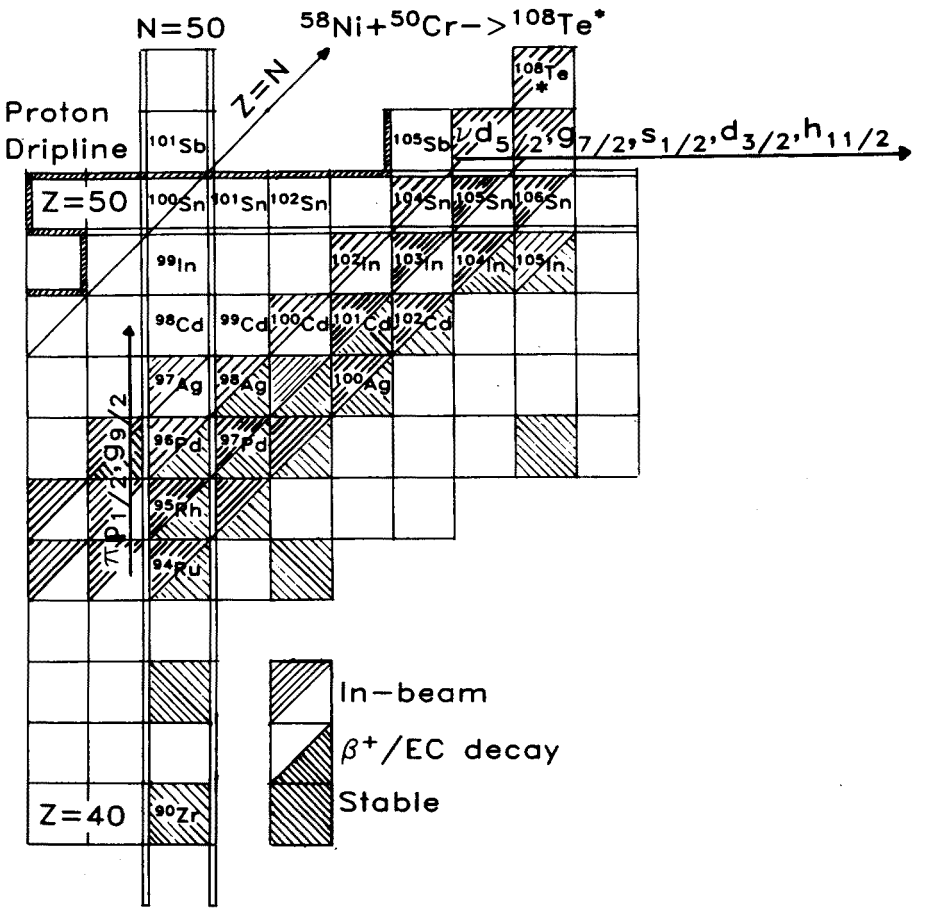

Fig. 1. Status of experimental approach to ^{100}Sn.

shown. It is landmarked by the key nuclei ^{95}Pd [3, 4] at $N = 49$, ^{97}Ag [5] and ^{96}Pd [6] at $N = 50$, the $T_z = 2$ nuclei ^{98}Ag [7], ^{100}Cd [8, 9], ^{102}In [10] and ^{104}Sn [11], and the lightest Sb isotopes ^{106,107}Sb [12].

The shell model analysis is based on earlier shell model studies [13, 14], the in-beam work done at OSIRIS and NORDBALL by the HMI [5–9,11], Göttingen [15–18], Gothenburg [4] and Uppsala [10, 12, 19] groups, and on β^+/EC studies by the GSI–Warsaw group [20, 21]. From the analysis the single particle structure at ^{100}Sn and information on the residual interaction can be deduced. At $N = Z$ the proton-neutron interaction is of specific interest, as the cooperative proton and neutron deformed shell gaps are predicted to give rise to a number of dramatic shape phenomena [22, 23]. A few examples from recent experiments are selected to demonstrate the pre-

dictive power of shell model calculations. Finally some future experiments will be discussed.

2. Experimental techniques

In-beam studies of neutron deficient nuclei following fusion evaporation reactions are characterized by small cross sections for neutron evaporation in the presence of predominant proton emission populating residues closer to stability. Typically some 30 nuclei are produced at the 1% level of the total residue cross section. This requires a highly selective setup including a powerful γ–array, implemented with efficient ancillary detectors for neutrons and charged particles. The most powerful device has been realized at NORDBALL [24] with efficiencies ϵ_γ=1.5% (at 662 keV), ϵ_n=25%, ϵ_p=65% and ϵ_α=45%. In Fig. 2 a recent development at OSIRIS is shown, which combines evaporation particle detection at the target with delayed γ-detection at a recoil catcher foil in the center of the γ-array [9, 32]. The detection sensitivity for isomers could thus be increased by more than an order of magnitude (see Sec. 3). Alternatively for prompt γ-emission the use of recoil mass separation (RMS) in conjunction with a charged particle ball, as realized at GASP [25], guarantees exit channel identification.

It has been shown by several authors that 4π detection efficiency for charged particles is highly desirable with at the same time as little as possible distortion of γ-ray detection [26, 27]. This restricts the possible detection

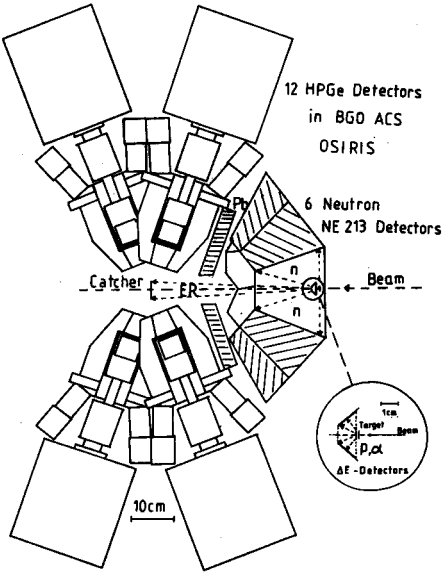

Fig. 2. Recoil catcher setup of OSIRIS

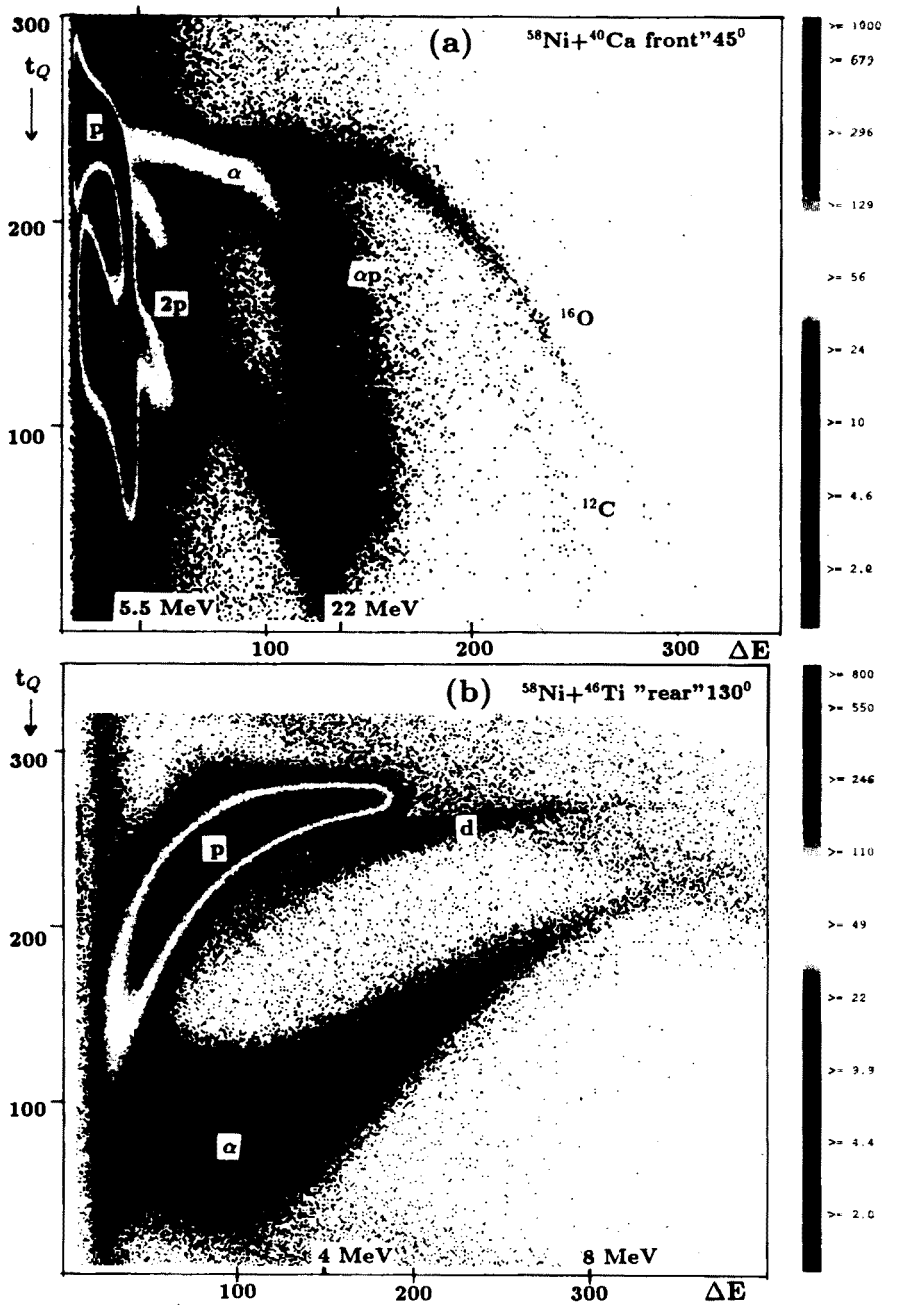

Fig. 3. Charge collection time t_Q vs. ΔE spectra in silicon surface barrier detectors for charged particles from the reactions of ^{58}Ni with ^{40}Ca at 45° measured with front side incidence (a) and with ^{46}Ti at 130° measured with rear side (low field) incidence (b).

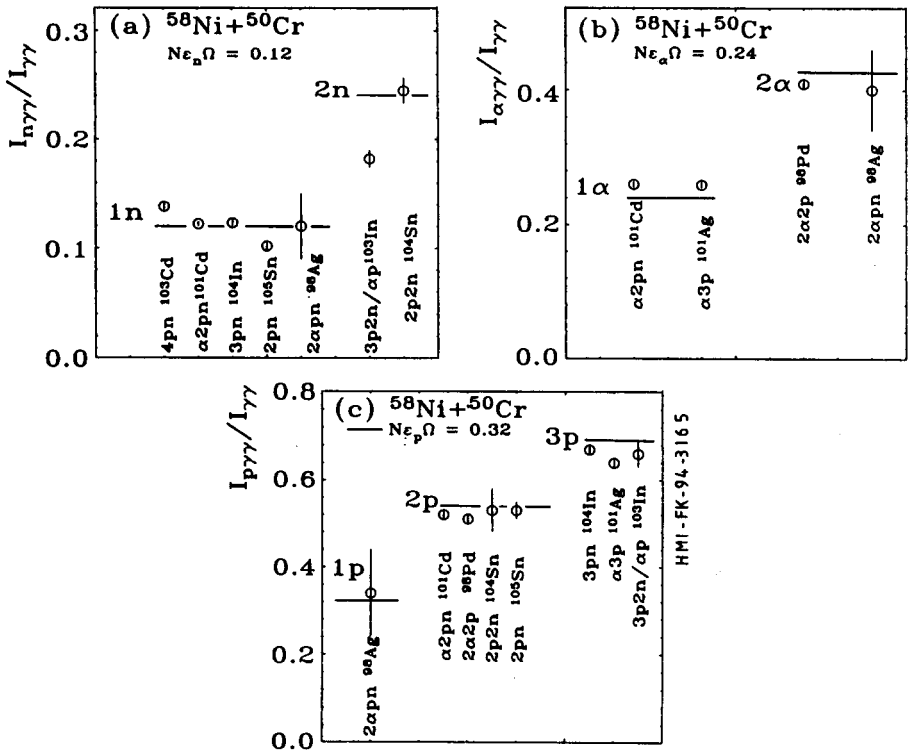

Fig. 4. Exit channel identification via ratios of $\gamma\gamma$ intensities with and without gating by neutrons (a), α–particles (b) and protons (c). The theoretical values for various multiplicities as calculated from the detection efficiencies are shown too.

technique to silicon surface barrier (SSB) detectors. It has been shown, that designs with virtually no γ-ray absorption can be found [25, 27, 28]. Exploiting pulse shape techniques and with rear side (low field) particle incidence [29, 30], a single self supporting shell of SSB detectors is sufficient. In Figs 3 (a), (b) spectra of the charge collection time t_Q vs. ΔE are shown for conventional (high field) and rear side incidence of particles for two different detectors, reactions and detection angles. Discrimination of protons and α particles is achieved over the full dynamic range in the latter case, whereas only limited improvement of the presently used ΔE technique is reached for conventional detection. The identification of unknown exit channels is accomplished by determining the multiplicity M of evaporated neutrons, protons and α particles. In Fig. 4 ratios of $\gamma\gamma$ coincidence intensities with and without particle gating are shown for the reaction ^{58}Ni+^{50}Cr at 250 MeV Ni beam energy. The values corresponding to different multiplicities

are well separated even for weak channels *e.g.* ^{98}Ag. The experimental ratios are also well reproduced by the multiplicity formula [31] adopting the measured efficiencies for neutrons, protons and α particles, which can be read from the M=1 values in Fig. 4. This is mainly due to the symmetric setup with identical detector positions (angles) and solid angles (see Fig. 2).

3. First results from a recoil catcher experiment at OSIRIS

We have used the setup shown in Fig. 2 to investigate isomeric decays in the range 15 ns $\leq t_{1/2} \leq$ 1 μs following the reaction ^{58}Ni+^{46,48}Ti at 230 MeV of the Ni beam from the "late" tandem-cyclotron combination of VICKSI. Residues recoiling from the 1.5 mg/cm^2 target (89% ^{46}Ti, 11% ^{48}Ti) were stopped in a 32 mg/cm^2 Nb catcher foil 40 cm downstream from the target. The Nb foils had an inner hole of 10 mm diameter for the scattered beam and were located in the center of OSIRIS. The 12 HPGe detectors in BGO Anti– Compton shields were used without collimators to suit the large source diameter of 50 mm. Filter detectors for neutrons (6 segments) and charged particles (4 segments) surrounded the target (Fig. 2). Catcher foils were exchanged every two hours by an automatic device [32] to avoid excessive background radiation from radioactivity.

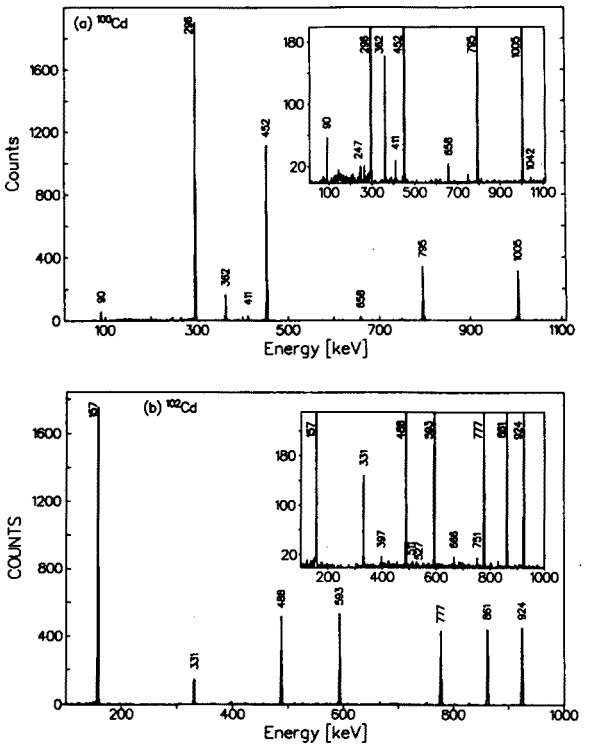

Fig. 5. Sum gate coincidence spectra for ^{100}Cd (n$\gamma\gamma$) (a) and ^{102}Cd (p$\gamma\gamma$) (b).

In Figs 5 (a), (b) neutron resp. proton gated sum coincidence spectra for the decay of the $I^{\pi} = 8^{+}$ isomers in ^{100,102}Cd are shown, which are populated in the ^{46,48}Ti(^{58}Ni,2p2n) reactions. The new transitions are enlarged in the inserts, where the peaks of previously known transitions are off-scale. The weakest observed γ-rays correspond to less than 1% of the strongest main cascade transitions, which indicates an improvement in detection sensitivity of over an order of magnitude in comparison to previous experiments [8]. The revised and improved decay schemes of the $I^{\pi}=8^{+}$ isomers in ^{100,102}Cd are shown in Figs 6, 7 in comparison to shell model predictions (see Sec. 4.2). The half lives have been measured, $t_{1/2} = 60(3)$ ns and 57(2) ns, respectively, for the two nuclei, in agreement with, but more accurate than, previous results [8, 33].

With the improved sensitivity and according to CASCADE predictions it should be possible to identify ^{98}Cd, which is populated *via* the α2n exit channel in the present experiment.

4. Shell model analysis

Numerous shell model calculations have been performed in the ($p_{1/2}$, $g_{9/2}$) proton (π) and neutron (ν) hole space [5, 6, 15–18]. They are based on the early work of Refs. [13, 14]. On the other hand, owing to its complexity, few attempts have been made in the neutron ν $d_{5/2}$, $g_{7/2}$, $s_{1/2}$, $d_{3/2}$, $h_{11/2}$ space [34–36]. Therefore in the present shell model approach the main emphasis was put on the $N \geq 50$ neutron particle space and its interaction with the firmly established proton hole space and the hardly investigated proton π $d_{5/2}$, $g_{7/2}$ particle orbitals [12]. It was the aim of the present work to describe the $N \geq 50$ nuclei around ^{100}Sn with one set of single particle energies, effective interactions and electromagnetic operators in a common model space. From the comparison with experimental data of key nuclei as close as possible to ^{100}Sn the shell model structure at the $N = Z = 50$ shell closure is inferred. To test the reliability of the extrapolation to ^{100}Sn in a few cases a restricted model space and alternative interactions are used. The shell model code RITSSCHIL was employed in this work [37].

4.1. Model space and effective interaction

In the present calculations a model space including the proton π $p_{1/2}$, $g_{9/2}$ and neutron ν $d_{5/2}$, $g_{7/2}$, $s_{1/2}$, $d_{3/2}$, $h_{11/2}$ orbitals was used. Occupation numbers of the $\nu h_{11/2}$ level was restricted to ≤ 2 or 3 for even and odd parity states, and the sum of particles in $\nu s_{1/2}$ and $d_{3/2}$ was ≤ 2. For the remaining orbitals occupation was not restricted. A ^{88}Sr core was assumed for $Z < 50$ nuclei and a ^{100}Sn core for $Z \geq 50$, *i.e.* core excitations of the

$N = 50$ neutron and the $Z = 50$ proton cores were not allowed. The two core nuclei were treated consistently, as for a given residual interaction the respective single particle (hole) energies are related by a simple relation [7, 38]. Therefore the experimental single particle energies (SPE) known for neutrons from transfer data on ^{88}Sr and ^{90}Zr targets [39] and for protons from previous shell model data [13, 14, 40] are used in the calculations. For the neutron $\nu s_{1/2}$, $d_{3/2}$, $h_{11/2}$ orbitals, which are not well determined by experimental data in $N = 51$ nuclei, adjustments were made from the analysis of Sn isotopes. The resulting values for a ^{100}Sn core are listed in Table I. The errors are given to indicate the uncertainties of the extrapolation from measured single particle energies to ^{100}Sn.

The $\pi\pi$ residual interaction is taken from Ref. [13] and the $\pi\nu$ and $\nu\nu$ interaction from a realistic set of two-body matrix elements (TBME) [34] except for $\pi g_{9/2}$ $\nu d_{5/2}$ and $\pi p_{1/2}$ $\nu(d_{5/2}, s_{1/2}, d_{3/2})$, where empirical values are known from ^{90}Y. TBME involving $\nu h_{11/2}$ were deduced from the Kuo–Herling set in ^{208}Pb [41] making use of the prescriptions given for (n, l, j) and A scaling [42] and the quenching of the $T = 1$ and $T = 0$ pairing TBME [43]. All unknown off-diagonal TBME were determined in a MSDI [44] fit to the known diagonal matrix elements of the respective multiplets, which guarantees phase consistency. For the Sn and Sb isotopes the schematic MSDI has been used as an alternative residual interaction with strength parameters $A_1 = 0.27$ MeV, $B_1 = 0.35$ MeV, $A_0 = 0.35$ MeV and $B_0 = -0.40$ MeV corresponding to $T = 1$ and $T = 0$ TBME. The monopole terms B were fitted to ground state binding energies.

Effective E2 charges $e_\pi = 1.72$ and $e_\nu = 1.44$ were taken from the ^{88}Sr region [45] and single particle g-factors from representative single particle states as compiled in Ref. [46].

4.2. Selected shell model results

To demonstrate the predictive power of the shell model analysis and to show the influence of alternative residual interactions, a few key examples are discussed below in comparison to recent experimental data.

^{100,102}*Cd*

The nucleus $^{100}_{48}Cd_{52}$ with two proton holes and two neutron particles outside ^{100}Sn can be regarded to be a key nucleus in the open $N > 50$, $Z < 50$ shell for two reasons. Due to the particle–hole character the $\pi\nu$ interaction is weak in stretched configurations and, hence, proton hole and neutron particle states coexist with little mutual distortion. In Fig. 6 the level scheme below the $I^\pi = 8^+$ isomer, which is known to be an almost pure $\pi(g_{9/2})^{-2}$ state [8], is compared to the shell model result normalized to the isomer excitation energy. The agreement is excellent, and indeed the shell model

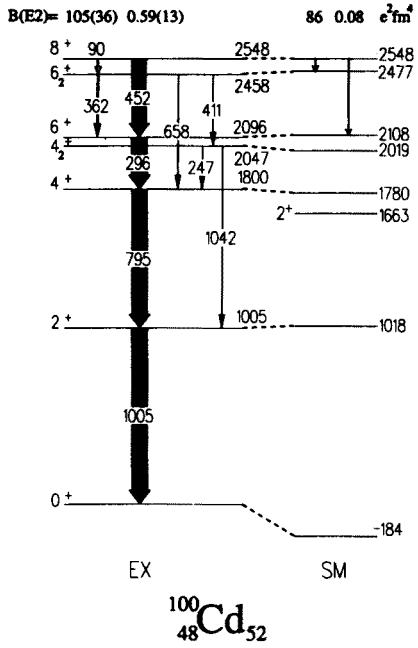

Fig. 6. Experimental and shell model level scheme for ^{100}Cd below the $I^\pi = 8^+$ isomer.

wave functions yield a 87%, 90% and 80% proton configuration for the 8^+, 6_2^+ and 4_2^+ states, whereas the 6_1^+ and 4_1^+ states are 84% and 82% neutron excitations. The 2^+ state is highly mixed as expected for non–aligned configurations. The strengths of the $B(\mathrm{E2}; 8^+ \rightarrow 6_2^+)$ and the hindrance of the $8^+ \rightarrow 6_1^+$ E2 transition (Fig. 6) are well reproduced, as are the branching ratios [9].

In conclusion realistic estimates for the $8^+ \rightarrow 6^+$ and $6^+ \rightarrow 4^+$ transition energies in ^{98}Cd and the $6^+ \rightarrow 4^+$ γ-ray in ^{102}Sn can be obtained. The inferred half lives of 0.5 μs for ^{98}Cd, $I^\pi = 8^+$ and 3 ns for ^{102}Sn, $I^\pi = 6^+$ may help to identify these nuclei in the data taken recently at OSIRIS and NORDBALL, respectively.

In Fig. 7 the corresponding experimental and theoretical level schemes of ^{102}Cd are shown. Again good agreement is found for level energies and B(E2) values. The purity of the wave functions is reduced due to the increased number of coupling possibilities for proton–neutron excitations.

^{98}Ag

The lighter $T_z = 2$ neighbour of ^{100}Cd, the $N = 51$ nucleus ^{98}Ag, has been studied in the β^+/EC decay of ^{98}Cd [20]. Recently high spin states were identified in-beam with the OSIRIS array in the ^{58}Ni+^{50}Cr reaction. The identification of the 2αpn exit channel is verified in Fig. 4. In Fig. 8 the

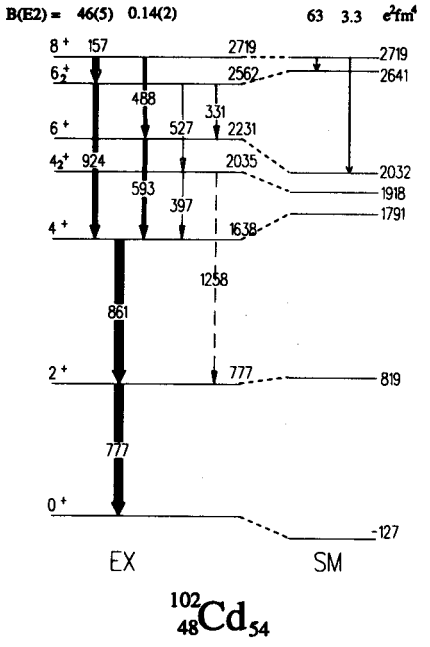

Fig. 7. Same as Fig. 6 for ^{102}Cd.

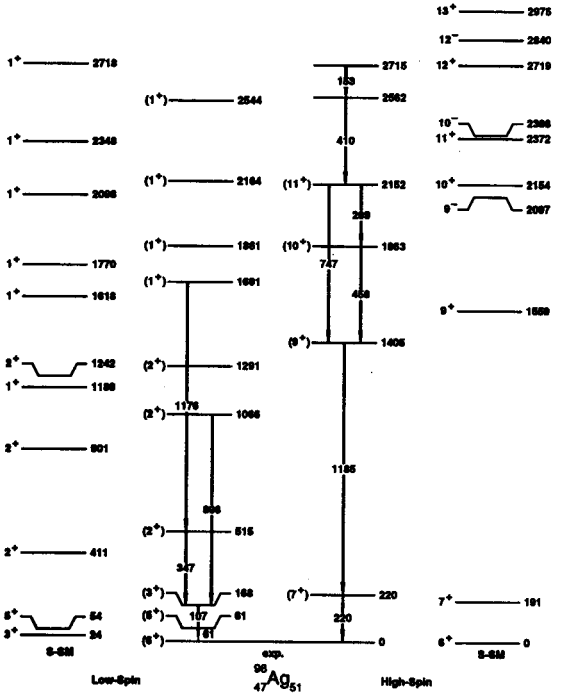

Fig. 8. Experimental and theoretical level schemes for low spin and high spin states in ^{98}Ag.

experimental low spin level scheme from the ^{98}Cd Gamow–Teller decay and the high spin levels are shown with the shell model predictions. The $N = 51$ nuclei are specifically sensitive to the neutron SPE and the average $\pi\nu$ interaction determining the SPE development from ^{91}Zr to ^{101}Sn [7, 47]. The $I^\pi = 1^+$ states and the Gamow–Teller distribution give evidence on the relative positions of the $\nu d_{5/2}$,$g_{7/2}$ orbitals and the $\pi g_{9/2}\nu(d_{5/2},g_{7/2})$ residual interaction. The good agreement found for the low spin [7] and the tentatively assigned high spin levels support the adequacy of the present shell model approach in extrapolating single particle neutron energies towards ^{100}Sn. Note that the theoretical odd parity levels shown in Fig. 8 are of $\pi p_{1/2}$ origin.

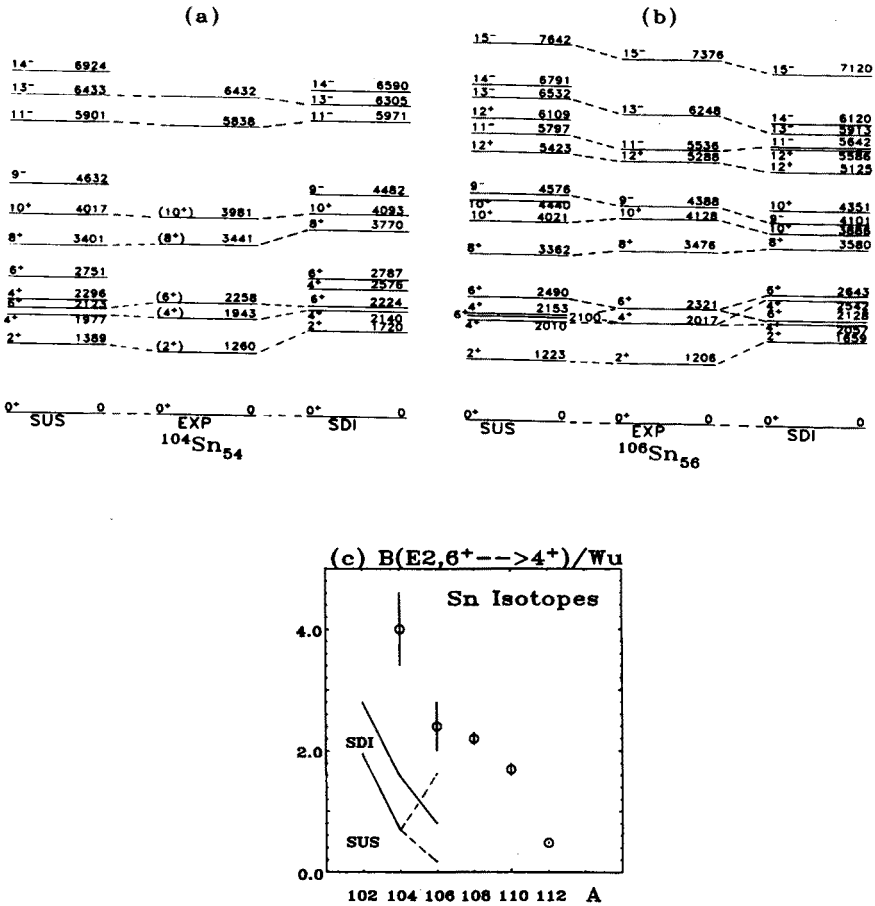

Fig. 9. Experimental and shell model level schemes for ^{104,106}Sn (a), (b) with two different interactions (see text) and $B(E2; 6^+ \rightarrow 4^+)$ in even Sn isotopes (c).

$^{104,106}Sn$

The $\nu\nu$ interaction can be best studied in the Sn isotopes. In Fig. 9 the $T_z = 2$ nucleus ^{104}Sn (a), and ^{106}Sn (b), where odd parity states are known, are compared to shell model predictions with two different residual interactions. Both, the realistic interaction implemented by empirical TBME and the MSDI reproduce the experimental levels equally well. Note the good agreement for odd parity states, which fixes the $\nu h_{11/2}$ single particle energy in ^{101}Sn. A major discrepancy is found for the $B(E2; 6^+ \rightarrow 4^+)$ in both interactions (Fig. 9 (c)), which for the MSDI could be improved with an reasonably increased effective neutron charge $e_\nu \simeq 2$ instead of the values given in Sec. 4.1. It should also be noticed, that in ^{106}Sn close lying yrare 6^+ and 4^+ states are calculated, that are connected by E2 strengths comparable to the experiment.

5. The shell model structure at ^{100}Sn

From the examples discussed in the preceding section and further evidence drawn from the study of ^{102}In [10], ^{103}In and ^{105}Sn [7] it can be concluded, that the residual interaction and single particle energies used in the present shell model approach give an adequate description of the semimagic and open shell nuclei between $N = 50$ and $Z = 50$. The single particle energies are summarized in Table I.

TABLE I

^{100}Sn single particle energies

	Neutrons	Protons
$p_{1/2}$	$-18.38(20)^a$	$-3.53(20)^a$
$g_{9/2}$	$-17.93(30)^a$	$-2.92(20)^a$
$d_{5/2}$	$-11.13(20)^b$	$+3.00(80)$
$g_{7/2}$	$-10.93(20)^b$	$+3.90(15)^c$
$s_{1/2}$	$-9.3(5)^b$	
$d_{3/2}$	$-9.2(5)^b$	
$h_{11/2}$	$-8.6(5)^b$	

[a] Ref. [14], [b] present work, [c] error relative to $d_{5/2}$ level.

For completeness the proton and neutron hole energies obtained from previous work [13, 14] and tested in many studies of $N \leq 50$ nuclei [5, 6, 15–18] are given, too. From a recent investigation of ^{106,107}Sb [12] first evidence on the unbound proton particle states in ^{100}Sn has been included.

The values are listed with error estimates to indicate the uncertainties in the extrapolation of SPE measured in ^{88}Sr and ^{90}Zr [39,40] to ^{100}Sn. In Fig. 10 these values are compared to predictions from Woods–Saxon and folded Yukawa potentials and a Skyrme III Hartree–Fock calculation [42]. Considerable deviations are observed for shell gaps, relative positions of neighbouring orbitals and absolute positions. It is therefore appropriate to check the extracted SPE with well known systematics of Coulomb energies [48] and spin–orbit splitting [49]. The Coulomb shift, as documented in the different ordinates for protons and neutrons in Fig. 10, is predicted to be 14.4 MeV [48] in good agreement with 14.1(6) and 14.9(4) MeV for $d_{5/2}$ particles and $g_{9/2}$ holes, respectively. The spin–orbit splitting for the l=4 levels determine the shell gaps. The extracted values of 6.9(6) MeV (protons) and 7.0(4) MeV (neutrons) agree well with the expected 7.1 MeV from systematics [49]. These intrinsic tests suggest that the uncertainties ar smaller than the conservative errors listed in Table I.

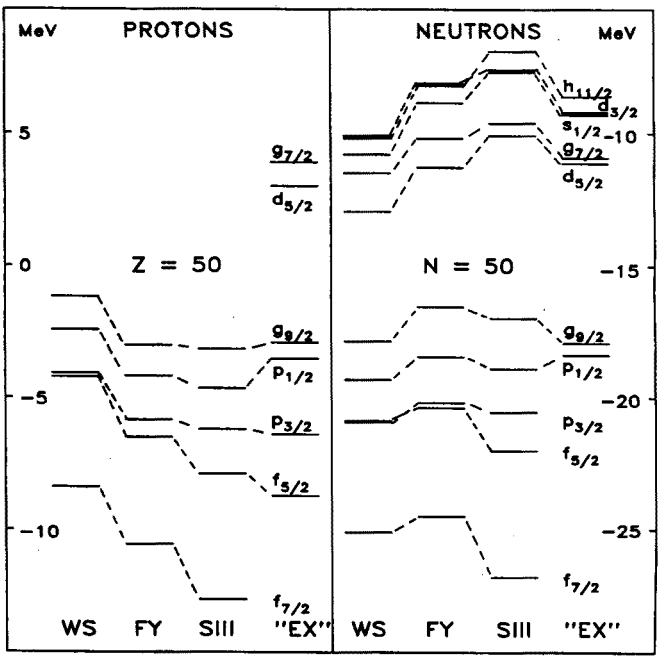

Fig. 10. Shell model extrapolated single particle energies for ^{100}Sn (EX)in comparison to predictions from Woods–Saxon (WS), folded Yukawa (FY) single particle model potentials and a Skyrme III (SIII) Hartree–Fock calculation [42].

6. Conclusion and prospect

With the available experimental and theoretical knowledge of the shell structure and residual interaction at the $N = Z = 50$ shell closure predictions can be made for so far non-identified or non-accessible nuclei even closer to ^{100}Sn. Their investigation will reduce the uncertainties of single particle energies and ambiguities in the residual interaction at this fix point of nuclear structure calculations.

As discussed in Section 4.2. the two–proton hole nucleus ^{98}Cd and its neutron particle $T_z = 1$ partner ^{102}Sn will provide a crucial test of the $\pi\pi$ and $\nu\nu$ interaction. Experiments have been performed at OSIRIS and NORDBALL and are in the course of analysis. The data should also provide information on ^{99}Cd and ^{103}Sn, which would fix the $\nu d_{5/2}$, $g_{7/2}$ and possibly $s_{1/2}$, $d_{3/2}$ and $h_{11/2}$ energies. So far little is known on the low spin orbitals $s_{1/2}$ and $d_{3/2}$, which could be best studied in the Gamow–Teller decay of the $\pi d_{5/2}$ ground states of the neutron deficient odd-A Sb isotopes.

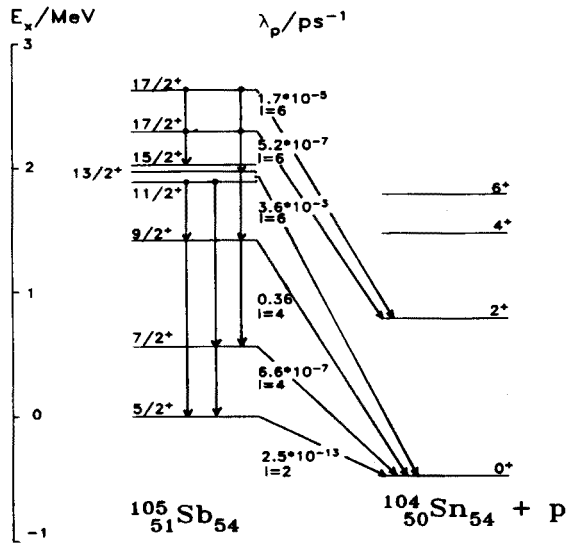

Fig. 11. Theoretical proton and γ decay scheme of the dripline nucleus ^{105}Sb.

Further evidence for the proton particle states, which are unbound for ^{100}Sn, can be obtained from ^{105}Sb, which recently has been reported to be a proton emitter [50]. An in-beam study would open the possibility to observe proton emission from excited states in competition with γ-decay. In Fig. 11 a theoretical decay scheme of ^{105}Sb is shown, calculated with the MSDI shell model approach discussed in Sect. 4.1. A simple WKB approach was used to estimate the decay widths λ_p [ps^{-1}] for proton decay

to ^{104}Sn, which are listed in Fig. 11. The calculations were normalized to reproduce the values assumed for ^{105}Sb [50], ^{109}I and ^{113}Cs [51]. There are obviously cases, where competition with γ-ray emission with $\lambda_\gamma \simeq 10^{-3} - 1$ is possible. Experimentally an efficient γ-array of the new generation in combination with 4π charged particle detection would be necessary. The recently proposed $N = 42$ Si-ball for EUROBALL [27] would provide an appropriate detection device. For the reaction ^{58}Ni+^{50}Cr a cross section of $\simeq 1$ mb is foreseen for the population of ^{105}Sb. Regarding future radioactive beam facilities the proton spectroscopy of dripline nuclei at rest might become an important spectroscopic tool.

The authors gratefully acknowledge the initiative of G. Pausch to exploit the pulse shape discrimination and appreciate the fruitful collaboration with their colleagues from the OSIRIS, NORDBALL and GASP collaborations.

REFERENCES

[1] K. Rykaczewski *et al.*, Proc. SELMA 94, Stockholm–Uppsala, to be published in *Phys. Scr.*
[2] R. Schneider *et al.*, *Z. Phys.* **A348** 241 (1994).
[3] E. Nolte *et al.*, *Z. Phys.* **A298**, 191 (1980).
[4] S.E. Arnell *et al.*, *Phys. Rev.* **C49**, 51 (1994).
[5] D. Alber *et al.*, *Z. Phys.* **A335**, 265 (1990).
[6] D. Alber *et al.*, *Z. Phys.* **A332**, 129 (1989).
[7] R. Schubart *et al.*, submitted to *Z. Phys.* **A**.
[8] D. Alber *et al.*, *Z. Phys.* **A344**, 1 (1992).
[9] M. Gorska *et al.*, *Z. Phys.* **A**, in press.
[10] D. Seweryniak *et al.*, *Z. Phys.* **A345**, 243 (1993).
[11] R. Schubart *et al.*, *Z. Phys.* **A340**, 109 (1991).
[12] D. Seweryniak *et al.*, *Phys. Lett.* **B321**, 323 (1994).
[13] D.H. Gloeckner, F.J.D. Serduke, *Nucl. Phys.* **A220**, 477 (1974).
[14] R. Gross, A. Frenkel, *Nucl. Phys.* **A267**, 85 (1976).
[15] M. Weiszflog *et al.*, *Z. Phys.* **A342**, 257 (1991).
[16] M.K. Kabadiysky *et al.*, *Z. Phys.* **A343**, 165 (1992).
[17] D. Rudolph *et al.*, *Phys. Rev.* **C49**, 66 (1994).
[18] D. Rudolph *et al.*,*Z. Phys.* **A342**, 121 (1992).
[19] A. Johnson *et al.*, *Nucl. Phys.* **A557**, 401c (1993).
[20] A. Plochocki *et al.*, *Z. Phys.* **A342**, 43 (1992).
[21] K. Rykaczewski, *Inst. Phys. Conf. Ser.* No.**132**, Sect. 5, 517 (1993).
[22] S. Aberg, *Nucl. Phys.* **A520**, 35c (1990).
[23] W. Nazarewicz, *Nucl. Phys.* **A520**, 333c (1990).
[24] G. Sletten in: Proc. Int. Seminar on Frontier of Nuclear Spectroscopy, Kyoto, October 1992, World Scientific, Singapore 1993.

[25] G. De Angelis, private communication.
[26] D. Seweryniak *et al.*, *Nucl. Instrum. Methods Phys. Res.* **A340**, 353 (1994).
[27] H. Grawe, Proposal for a 4π silicon ball for EUROBALL, unpublished.
[28] W. Bohne, *et al.*, *Ann. Rep. 1991, HMI-B* **497**, 92 (1992); *Ann. Rep. 1992, HMI-B* **507**, 79 (1993).
[29] G. Pausch *et al.*, *Nucl. Instrum. Methods Phys. Res.* **A332**, 43 (1992); **A337**, 573 (1994).
[30] G. Pausch *et al.*, *Nucl. Instrum. Methods Phys. Res.*, in press.
[31] D. Habs *et al.*, Lawrence Berkeley Laboratory, USA, Preprint PUB-5020, 1979.
[32] R. Schubart *et al.*, Proc. SELMA 94, Stockholm–Uppsala, to be published in *Phys. Scr.*
[33] W.F. Piel *et al.*, *Phys. Rev.* **C37**, 1067 (1988).
[34] L.D. Skouras, C. Dedes, *Phys. Rev.* **C15**, 1873 (1977).
[35] T. Engeland *et al.*, *Phys. Rev.* **C48**, R535 (1993).
[36] B.A. Brown, private communication.
[37] D. Zwarts, *Comput. Phys. Commun.* **38**, 365 (1985).
[38] J. Blomqvist, R. Rydström, *Phys. Scr.* **31**, 31 (1985).
[39] H.P. Blok *et al.*, *Nucl. Phys.* **A273**, 142 (1976).
[40] K.T. Knöpfle *et al.*, *Nucl. Phys.* **A159**, 642 (1970).
[41] T.T.S. Kuo, G.H. Herling, Naval Res. Lab., Washington, NRL Memorandum Report 2258 (1971).
[42] G. Leander *et al.*, *Phys. Rev.* **C30**, 416 (1984).
[43] W.T. Chou, E.K. Warburton, *Phys. Rev.* **C45**, 1720 (1992).
[44] P.J. Brussaard *et al.*, *Nucl. Phys.* **A102**, 593 (1967).
[45] P. Raghavan *et al.*, *Phys. Rev. Lett.* **54**, 2592 (1985).
[46] P. Raghavan *et al.*, *At. Data Nucl. Data Tables* **42**, 189 (1989).
[47] H. Grawe *et al.*, *Progr. Part. Nucl. Phys.* **28**, 281 (1992).
[48] J. Jänicke in: *Isospin in Nuclear Physics*, ed. D.H. Wilkinson, North-Holland, Amsterdam 1969, p.336.
[49] G. Mairle, *Phys. Lett.* **B304**, 29 (1993).
[50] R.J. Tighe *et al.*, *Phys. Rev.* **C49**, R2871 (1994).
[51] S. Hofmann in: *Particle Emission from Nuclei*, eds M. Ivascu, D.N. Poenaru, CRC Boca Raton, FL 1989, vol. 2, chap. 2.